S0019-1035(03)00404-4/FLA AID:7281 Vol.●●●(●●●)
ELSGMLTM(YICAR):m5 2004/01/13 Prn:26/01/2004; 9:41

yicar7281

P.1 (1-10)
by:Jolanta p. 1

Available online at www.sciencedirect.com

SCIENCE DIRECT®

Icarus ●●● (●●●●) ●●●–●●●

ICARUS

www.elsevier.com/locate/icarus

A technique for calculating meteor plasma density and meteoroid mass from radar head echo scattering

S. Close,[a,b,*] M. Oppenheim,[b] S. Hunt,[a,b] and A. Coster [a]

[a] *MIT Lincoln Laboratory, 244 Wood Street, Lexington, MA, USA*
[b] *Boston University, Center for Space Physics, Boston, MA, USA*

Received 21 April 2003; revised 23 November 2003

Abstract

Large-aperture radars detect the high-density plasma that forms in the vicinity of a meteoroid and moves approximately at its velocity; reflections from these plasmas are called head echoes. To determine the head plasma density and configuration, we model the interaction of a radar wave with the plasma without using assumptions about plasma density. This paper presents a scattering method that enables us to convert measurements of radar cross-section (RCS) from a head echo into plasma density by applying a spherical scattering model. We use three methods to validate our model. First, we compare the maximum plasma densities determined from the spherical solution using 30 head echoes detected simultaneously at VHF and UHF. Second, we use a head echo detected simultaneously at VHF, UHF and L-band to compare plasma densities at all frequencies. Finally, we apply our spherical solution to 723 VHF head echoes and calculate plasma density, line density and meteoroid mass in order to compare these values with those obtained from a meteoroid ablation and ionization model. In all three comparisons, our results show that the spherical solution produces consistent results across a wide frequency range and agrees well with the single-body ablation model.

Keywords: Meteors; Meteoroids; Radar; Radio observations

1. Introduction

Meteoroids entering the Earth's atmosphere ablate and form plasma between approximately 140 and 70 km altitude. These plasmas are detectable by radar and have been categorized into the specular trail, the nonspecular trail, and the head echo. Specular trails occur when the radar beam lies perpendicular to a meteoroid's trajectory and the meteoroid plasma fills successive Fresnel zones. Nonspecular trail returns occur when a meteoroid travels quasi-parallel to the radar beam and forms field-aligned-irregularities. Head echoes are returns from the plasma immediately surrounding the meteoroid that moves approximately at the meteoroid's velocity, which we will refer to herein as head plasma.

Head echoes have been detected for many decades (McKinley and Millman, 1949), however a comprehensive description of these phenomena is still lacking. Recent progress has been achieved through the use of high-power radars such as Arecibo (Mathews et al., 1997; Janches et al., 2000; Zhou et al., 1998), EISCAT (Pellinen-Wannberg and Wannberg, 1994; Pellinen-Wannberg et al., 1998), Jicamarca (Chapin and Kudeki, 1994), the Millstone Hill Radar, (Evans, 1966), (Erickson et al., 2001) and ALTAIR (Close et al., 2000). In Close et al. (2002b) we showed that head plasma formation is highly-dependent upon altitude and velocity and that the reflection from the plasma suggests at an object with a spherical cross-section. The head plasma density was believed to decrease with distance from the meteoroid with a peak plasma frequency near the incident radar frequency.

In this paper, we expand upon our scattering model by abandoning assumptions relating to plasma density and model the interaction of a radar wave with head plasma by solving the wave equation. The resulting reflection coefficient can therefore be applied to head plasmas with plasma frequencies either above or below the radar frequency.

Section 2 gives a brief overview of the high-resolution, multi-frequency ALTAIR head echo data set. Section 3 gives an overview of our spherical scattering calculations. Sec-

* Corresponding author.
E-mail address: sigrid@ll.mit.edu (S. Close).

0019-1035/$ – see front matter
doi:10.1016/j.icarus.2003.11.018

tion 4 describes methods used to validate the spherical solution. Section 5 summarizes and expands upon future work.

2. ALTAIR head echo data

ALTAIR is a 46-m diameter, high-power, two-frequency radar operating at 160 MHz (VHF) and 422 MHz (UHF), which resides in the central Pacific at 9° N and 167° E (geographic) on the island of Roi-Namur in the Kwajalein Atoll, Republic of the Marshall Islands. ALTAIR transmits a peak power of 6 MW simultaneously at the two frequencies with right-circularly (RC) polarized signal energy in a half-power beamwidth of 2.8° and 1.1° at VHF and UHF, respectively. ALTAIR receives both right-circular and left-circular energy and has four additional receiving horns for the purpose of angle measurement, which gives the position of an object in three dimensions.

Radar meteor data were collected at KMR on November 18, 1998, during a 4-h period in 2-min segments, which was designed to span the predicted peak of the Leonid storm (07:30 AM local time). Four radars, including ALTAIR, TRADEX (L- and S-band), ALCOR (C-band) and MMW (Ka- and W-band) were pointed simultaneously on and off-radiant. The ALTAIR data, which are used in this study, showed a peak detection rate of 1.6 VHF head echoes every second (Close et al., 2002a). Amplitude and phase data were recorded for each frequency and four receiving channels for altitudes spanning 70–140 km at VHF and 90–110 km at UHF. The UHF altitude extent was smaller due to the very small (7.5 m) range sample spacing and the corresponding limit on disk space. The two ALTAIR waveforms used to collect the data were a 40 μs VHF chirped pulse (30 m range spacing), and a 150 μs UHF chirped pulse (7.5 m range spacing). A 333 Hz pulse-repetition frequency (PRF) was utilized for its high sampling rate, which allows the calculation of 3D velocity as a function of altitude. Using these waveforms, ALTAIR can detect a target as small as −55 decibels-relative-to-a-square-meter (dBsm) at VHF and −75 dBsm at UHF at a range of 100 km.

3. Spherical scattering solution

The scattering from a sphere with a uniform dielectric constant has been given by Mie (1912), and Stratton (1941), and the scattering solution of an electromagnetic wave from a cylindrical meteor trail with a nonuniform dielectric constant has been given by Kaiser and Closs (1951); Jones and Jones (1991); and Poulter and Baggaley (1977). We combine these methods to calculate the scattering from head plasma and assume the following:

(1) The reflecting component of head plasma can be approximated as spherically symmetric.
(2) The head plasma's radius depends upon altitude and scales with the atmospheric mean free path and meteoroid speed.
(3) The head plasma density behaves as a Gaussian function.

Our goal is to take the measured ALTAIR head echo RCS data and determine peak head plasma density.

3.1. Head plasma model

Head echo RCS depends upon the density and the size of the head plasma distribution. We choose this distribution using a physically plausible approximation and then derive the expected head plasma density using this distribution and the measured RCS with our scattering equations.

Our approximation of the head plasma density, $n(r)$, is a Gaussian function, or

$$n(r) = n_{\max} \exp\left(-(r/r_{\max})^2\right), \tag{1}$$

where $n_{\max}$ is the maximum plasma density for each head plasma (near the meteoroid's position at the center of the head plasma), r is the radial distance from the center of the head plasma, and $r_{\max}$ defines what we call the "physical size" of the head plasma.

We expect the physical size of head plasma, $r_{\max}$, to scale approximately with the atmospheric mean free path for two reasons. First, the meteoroid principally emits neutral gas, some of which ionizes after colliding with neutral molecules, freeing the electrons measured by radar. Hence, as the mean free path decreases, so will the size of the ionized region. Second, the gas and plasma released from a meteoroid expands largely without deflection until it reaches, on average, a distance roughly equaling the mean free path; at this point, it will expand at a slower diffusive rate. The transition distance is called the initial radius. For specular trails, this distance has been estimated as approximately twenty times the atmospheric mean free path (M. Campbell, private communication), which can also be adjusted to incorporate the speed of the meteoroid (Jones, 1995). However, since the head plasma is undoubtedly much smaller than the initial trail radius, we scale the Jones formula linearly. We validated this scaling by using the simultaneous VHF/UHF detections, which will be discussed further in Section 4. Based on our observations and calculations, we choose our head radius, $r_{\max}$, to be 0.023 times the Jones formula or

$$r_{\max} = 0.023(2.845 \times 10^{18} v^{0.8}/n), \tag{2}$$

where v is the 3D speed of the head echo in km s^{-1} and n is the background number density at the head echo detection altitude in m^{-3}. The number 0.023 was determined by using the ALTAIR head echoes that were detected simultaneously at VHF and UHF. Specifically, we converted head echo RCS to peak plasma density using the scattering model discussed in Sections 3.2 and 3.3. We then compared the peak plasma density derived using the VHF RCS measurement with the

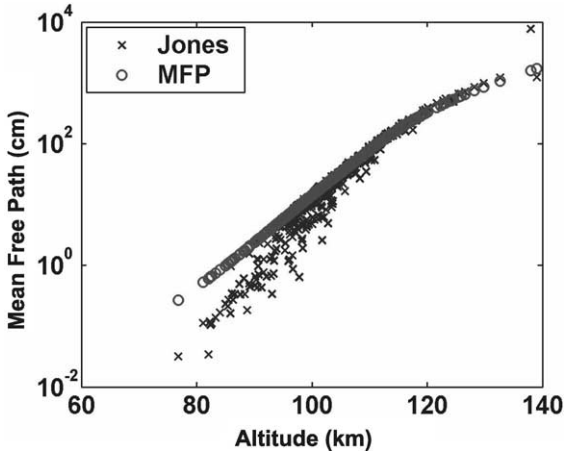

Fig. 1. Plot of modified Jones formula applied to ALTAIR head echo data collected during the Leonid 1998 shower. These data include the maximum velocity and maximum altitude from each of the measured 723 VHF head echoes.

peak plasma density derived using the UHF RCS measurement for the same head echo. We subsequently varied the head radius, $r_{\max}$, until the two plasma densities output from the scattering model matched at both VHF and UHF.

We refer to Eq. (2) as the modified Jones formula. At high altitudes (> 105 km), Eq. (2) is approximately one atmospheric mean free path; at lower altitudes, Eq. (2) will produce head radii that are slightly smaller than a mean free path. A comparison of the modified Jones' formula with one atmospheric mean free path is contained in Fig. 1. These data include 723 head echoes detected at VHF during the Leonid 1998 shower, where each point represents the maximum altitude and maximum velocity from each head echo streak. These data show the dependence of speed on altitude, which was noted in Close et al. (2002b).

The dielectric constant varies as

$$\frac{\varepsilon(r)}{\varepsilon_0} = 1 - \frac{\omega_p^2}{\omega^2} = 1 - \frac{n(r)e^2}{\varepsilon_0 m\omega^2}, \tag{3}$$

where ε_0 is the permittivity in free space, ω_p is the plasma frequency, ω is the radar frequency, e is the electron charge, m is the electron mass, and $n(r)$ is the plasma density defined by Eq. (1). Both the $\vec{v} \times \vec{B}$ component of the Lorentz force due to the motion in the geomagnetic field, $\vec{B}$, as well as any collisional terms can be neglected, since both the gyrofrequency and the collisional frequency in the E-region are negligible compared to the VHF and UHF frequencies, and the field is not high enough to drive electrons to relativistic speeds.

3.2. Scattering model

We begin our spherical scattering calculation by using an incident plane wave polarized in the x-direction, propagating in the z-direction, and incident upon spherical plasma (head plasma) embedded in a homogeneous medium. The incident plane wave in the radial direction may be represented by

$$\vec{E}_{\text{inc}}(z,\omega) = \hat{a}_x E_0 e^{-ikz-i\omega t} = \hat{a}_x E_0 e^{-ikr\cos\theta - i\omega t}, \tag{4}$$

where $k = \omega/c$, r is the radius vector, ω is the frequency and $\hat{a}_x$ is the direction vector given by

$$\hat{a}_x = \sin\theta\cos\varphi\,\hat{i} + \cos\theta\cos\varphi\,\hat{j} - \sin\varphi\hat{k}, \tag{5}$$

where θ and φ are the spherical angles and $\hat{i}$, $\hat{j}$ and $\hat{k}$ are unit vectors. We expand the incident wave in terms of spherical harmonics by using the wave transformation

$$e^{ikr\cos\theta} = \sum_{n=0}^{\infty} i^n (2n+1)\, j_n(kr)\, P_n(\cos\theta), \tag{6}$$

where j_n is the nth order Bessel function of the first kind and $P_n(\cos\theta)$ is the nth order Legendre function.

The time-independent incident electric field is now characterized using spherical Bessel functions, and in the radial direction is given by

$$E_{r\_\text{inc}} = E_0 \sin\theta\cos\varphi e^{-ikr\cos\theta} = E_0 \frac{\cos\varphi}{ikr}\frac{\partial}{\partial\theta}(e^{-ikr\cos\theta}), \tag{7}$$

which becomes

$$E_{r\_\text{inc}} = -\frac{iE_0\cos\varphi}{kr}\sum_{n=1}^{\infty} i^n (2n+1)\, j_n(kr)\, P_n^1(\cos\theta), \tag{8}$$

where is $P_n^1(\cos\theta)$ the associate Legendre function; we now start the summation with $n = 1$ because $P_0^1(\cos\theta) = 0$. Likewise, the time-independent reflected electric field in the radial direction becomes

$$E_{r\_\text{ref}} = -\frac{iE_0\cos\varphi}{kr}\sum_{n=1}^{\infty} i^n R_n (2n+1) h_n^1(kr)\, P_n^1(\cos\theta), \tag{9}$$

where R_n is the reflection coefficient, and h_n^1 is the nth order Hankel function of the first kind. The penetrating electric field inside the head plasma in the radial direction is given by

$$E_{r\_\text{pen}} = -\frac{iE_0\cos\varphi}{k_p r}\sum_{n=1}^{\infty} i^n c_n (2n+1)\, j_n(k_p r)\, P_n^1(\cos\theta), \tag{10}$$

where k_p is the wavelength associated with the head echo plasma, and c_n is a coefficient associated with the field inside the head plasma.

The total field external to the head plasma, $E_{r\_\text{ext}} = E_{r\_\text{inc}} + E_{r\_\text{ref}}$, now using the Hankel function of the second kind, is

$$E_{r\_\text{ext}} = -\frac{iE_0\cos\varphi}{kr}\sum_{n=1}^{\infty} i^n P_n^1(\cos\theta)(2n+1) \times \Big(j_n(kr) + R_n\big(2j_n(kr) - h_n^2(kr)\big)\Big). \tag{11}$$

We can write Eq. (11) as a transverse potential, V_{ext}, using the electric field components in spherical coordinates as described by Wyatt (1962) and Stratton (1941) or

$$V_{\text{ext}} = \frac{E_0 k \cos\varphi}{\omega} \sum_{n=1}^{\infty} \frac{i^n (2n+1) P_n^1(\cos\theta)}{n(n+1)} \times \Big(j_n(kr) + R_n \big(2 j_n(kr) - h_n^2(kr)\big)\Big). \quad (12)$$

For a sphere with a uniform dielectric constant, we can solve for the reflection coefficient and c_n by equating the sum of the incident and reflected electric (and magnetic) fields (Eq. (11)) with the penetrating field (Eq. (10)). In other words, a single transition radius means the fields are continuous at $r = r_{\max}$ and will produce the typical Mie scattering curve for a sphere with an arbitrary size and an incident radar wave of arbitrary wavelength. However, because we have head plasma with a dielectric constant that depends upon radial distance from the meteoroid, we cannot use a uniform dielectric constant in Eq. (10). Our approach will be to compare the form of the potential in Eq. (12) with the electrostatic solution, derived from Laplace's equation, in order to solve for the head plasma density.

We now consider Laplace's equation in order to determine how the electrostatic potential varies as a function of radial distance from the center of the head plasma. For a spherical plasma distribution with a dielectric constant dependent upon r, Laplace's equation is given by

$$\vec{\nabla} \cdot (\varepsilon \vec{\nabla} V) = \vec{\nabla}\varepsilon \cdot \vec{\nabla} V + \varepsilon \nabla^2 V = 0, \quad (13)$$

where ε is the head plasma's dielectric constant and V is the potential. In spherical coordinates, the potential function is

$$V = \cos\phi \sum_{n=1}^{\infty} V_n P_n^1(\cos\theta), \quad (14)$$

where V_n is the solution of the radial component of Laplace's equation, or

$$\frac{\mathrm{d}}{\mathrm{d}r}\left(\varepsilon r^2 \frac{\mathrm{d}V_n}{\mathrm{d}r}\right) = n(n+1)\varepsilon V_n. \quad (15)$$

The solution to Eq. (15) in regions of constant ε is given by

$$V_n = A_n r^n + B_n r^{-(n+1)}, \quad (16)$$

where A_n and B_n are coefficients determined by boundary conditions.

Equation (15) gives a solution to the full electromagnetic wave system when the dominant scattering mechanism results from electrostatic scattering in a manner similar to that described for cylindrical meteor trail scattering by Kaiser and Closs (1951). Assuming Maxwell's equations, the linearized plasma fluid continuity equation, and Lorentz equation, Wyatt (1962) showed that an equation describing the radial potential can be written as

$$V_n'' + V_n'\left(\frac{2}{r} - \frac{\varepsilon'}{\varepsilon}\right) + V_n\left(k^2 - \frac{\varepsilon'}{\varepsilon r} - \frac{n(n+1)}{r^2}\right) = 0, \quad (17)$$

where the prime denotes differentiation with respect to r. This applies even in the case of zero-order plasma density gradients, which is expected for head plasmas. Therefore, if we stipulate that $|(kr)^2 - r\varepsilon'/\varepsilon| \ll n(n+1)$, then Eqs. (17) and (15) have the same form. This assumption limits us to cases where the radar wavelength is greater than the size of the head plasma.

To obtain the reflection coefficient, R_n, we combine Eqs. (14) and (16) and compare the result to Eq. (12), giving

$$-\frac{1}{R_n} \cong 2 - \frac{n h_n^2(kr) A_n r^{2n+1}}{(n+1) j_n(kr) B_n}. \quad (18)$$

Equation (15) has two singularities which we must address, including at the center of the head plasma ($r = 0$), as well as where $\varepsilon = 0$, which we will define to be at $r = r_0$. The singularity at the center can be dealt with by requiring that V_n be well-behaved at the origin; the singularity at the boundary ($\varepsilon = 0$) requires complex integration because the dielectric constant can be negative inside the head plasma but positive outside, which means that it passes through a zero point. We can address this singularity by considering a thin region (smaller than a radar wavelength) at $r = r_0$ and setting $x = r^n$ in Eq. (15) to give

$$\frac{\mathrm{d}}{\mathrm{d}x}\left(\varepsilon \frac{\mathrm{d}V_n}{\mathrm{d}x}\right) = -\frac{(n+1)}{n}\varepsilon \frac{\mathrm{d}}{\mathrm{d}x}\left(\frac{V_n}{x}\right), \quad (19)$$

which in this region is approximately

$$\frac{\mathrm{d}}{\mathrm{d}x}\left(\varepsilon \frac{\mathrm{d}V_n}{\mathrm{d}x}\right) = -\frac{(n+1)}{n}\frac{\varepsilon}{r_0^n}\frac{\mathrm{d}V_n}{\mathrm{d}x} \quad (20)$$

meaning

$$\varepsilon \frac{\mathrm{d}V_n}{\mathrm{d}x} \approx \text{const} = C_n \quad \text{or} \quad \varepsilon \frac{\mathrm{d}V_n}{\mathrm{d}r} \approx C_n \quad (21)$$

when $|r - r_0| \ll r_0$. To solve this differential equation, we use the form of the plasma density given in Eq. (1) and expand the corresponding dielectric constant in a power series around $(r - r_0)$, such that

$$\varepsilon = (r - r_0)\varepsilon'(r_0), \quad (22)$$

where ε' is the derivative of ε at $\varepsilon = 0$. The physical significance of $\varepsilon' r_0$ corresponds to the value ε would have at the center of the head plasma if the gradient of ε in the thin boundary region had been continued into the center of the head plasma. We then use contour integration on Eq. (21) to obtain

$$V_{nB} - V_{nA} = \frac{C_n}{\varepsilon'(r_0)}\left[\ln\left|\frac{\varepsilon_B}{\varepsilon_A}\right| + i\pi\right], \quad (23)$$

where V_{nA} and ε_A are the potential and dielectric constant inside the head plasma, and V_{nB} and ε_B are the potential and dielectric constant outside of the head plasma.

3.3. Numerical and approximate analytical solutions

We must still solve for the constants A_n and B_n in Eq. (18), which can be determined either numerically or analytically. Using the numerical technique of Kaiser and Closs (1951), we can integrate Eq. (15) using a piecewise linear approximation and solve for the potential at each increment. We begin the integration by assuming that $\varepsilon' = 0$ when $r \ll 1$, making $V = Ar$ at the center of the head plasma ($r = 0$). Therefore, we set $V = 0$ and $V' = 1$ at $r = 0$, since the ratio of the coefficients (A_n/B_n) in the final reflection coefficients is independent of our initial value of A at the center of the head plasma. If the head plasma has a high peak plasma density, such that the dielectric constant passes through a singularity at $\varepsilon = 0$, we use Eq. (23) in the vicinity of the singularity to solve for the potential. We subsequently integrate out to where the ratio A_n/B_n stops changing near $\varepsilon = 1$.

In order to derive an analytical solution for the ratio A_n/B_n, we invoke the Herlofson model described in Herlofson (1951), which is an approximation to our dielectric constant (Eqs. (3) and (1)), which is shown in Fig. 2a. The Herlofson approximation is shown in Fig. 2b and will now be used to solve for the constants A_n and B_n analytically. Herlofson (1951) and Kaiser and Closs (1951) developed this method in cylindrical coordinates to characterize scattering from a meteor trail, and we apply their techniques to head echo scattering by changing their equations to accommodate a spherical coordinate system.

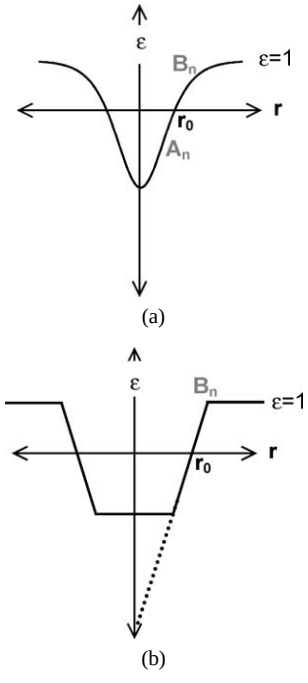

Fig. 2. (a) Illustration of the dielectric function resulting from using a Gaussian density distribution (Eq. (1)), and (b) the Herlofson approximation to this model, where the head plasma is modeled as a homogeneous plasma at its center with a thin region of increasing dielectric constant (decreasing density) at its edge.

Within the homogeneous region (A_n in Fig. 2b), we set $V_{nA} = r^n$ which allows us to solve for the constant in Eq. (21), $C_n = \varepsilon n r_0^{n-1}$, the potential in Eq. (23), V_{nB}, and also the derivative of the potential with respect to r, V'_{nB}, or

$$V_{nB} = r_0^n + \frac{n\varepsilon r_0^n}{r_0 \varepsilon'(r_0)}\big[-\ln|\varepsilon_A| + i\pi\big], \tag{24}$$

$$r_0 V'_{nB} = n\varepsilon_A r_0^n. \tag{25}$$

We solve for the coefficients A_n and B_n by comparing Eq. (16) and the derivative of the potential in Eq. (16) at $r = r_0$

$$V_{nB} = A_n r_0^n + B_n r_0^{-(n+1)}, \tag{26}$$

$$r_0 V'_{nB} = nA_n r_0^n - (n+1) B_n r_0^{-(n+1)} \tag{27}$$

with Eqs. (24) and (25). Specifically, we add and subtract Eq. (24) with Eq. (26), and Eq. (25) with Eq. (27) to solve for the coefficients, which gives

$$\frac{A_n}{B_n} = \frac{(n+1)}{n r_0^{2n+1}} \frac{\left(1 + \frac{\varepsilon_A n}{n+1} + \frac{\varepsilon_A n}{\varepsilon'(r_0) r_0}(i\pi - \ln|\varepsilon_A|)\right)}{\left(1 - \varepsilon_A + \frac{\varepsilon_A n}{\varepsilon'(r_0) r_0}(i\pi - \ln|\varepsilon_A|)\right)}, \tag{28}$$

where ε_A is a constant. The mode (n) to which we must sum depends upon the altitude (head plasma radius) and the incident wavelength.

Finally, we relate the measured scattering cross-section, σ_{meas}, to the reflection coefficient using

$$\sigma_{\text{meas}} = \sum_n \frac{\lambda^2 (n + 1/2)^2}{\pi} |R_n|^2, \tag{29}$$

where λ is the radar wavelength (Jackson, 1975; Morse and Feshbach, 1953) and σ_{meas} is the measured ALTAIR head echo RCS. The spherical reflection coefficient, using Eqs. (18) and (28), is converted to cross-section, σ_{meas}, using Eq. (29) and plotted as a function of $r_{\max}$ and plasma frequency in Fig. 3 for a theoretical array of plasma frequencies (plasma densities) detected using the VHF frequency. When the plasma frequency approaches the radar frequency, the cross sections approach 0 dBsm for large radii, which is intuitive. Note the enhanced color near the VHF wavelength (1.87 m), which we believe results from the similarity to Mie scattering. Mie scattering produces constructive and destructive interference from a metal sphere with a diameter that is a multiple of the radar wavelength.

4. Scattering theory validation

We validate the spherical scattering solution using the ALTAIR data set. Specifically, we apply our calculations to the measured RCS observations in order to calculate peak head plasma density. The head echo RCS observations are highly dependent on radar frequency, however the head plasma density is not. Therefore, if we obtain the same

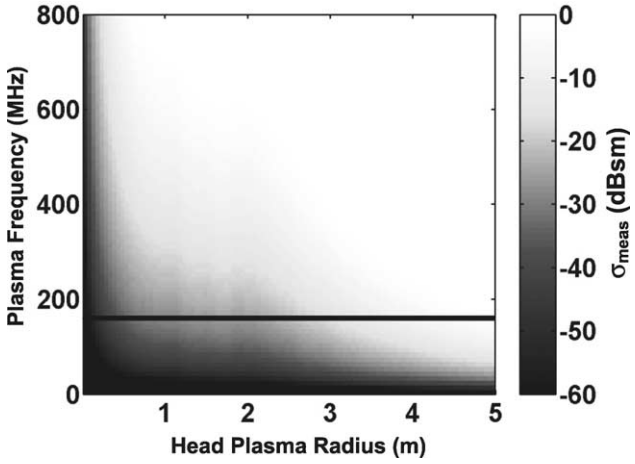

Fig. 3. VHF head echo cross-section in dBsm as a function of maximum head plasma frequency and head plasma radius. Head echo cross-sections are derived by calculating the head echo reflection coefficients using the scattering equations. The solid line corresponds to the frequency of the VHF radar (160 MHz).

head plasma density using simultaneous multi-frequency observations, we can claim that our scattering theory is self-consistent.

We use three methods to validate our theory. First, we compare the maximum head plasma densities, derived using our spherical scattering solution, of 30 head echoes detected simultaneously at VHF and UHF. We also examine the head plasma density dependence on altitude. Second, we compare the maximum head plasma density for a head echo detected simultaneously at VHF, UHF and L-band using the ALTAIR and TRADEX radars. Third, we calculate maximum head plasma density and convert density to line density and meteoroid mass for 723 VHF head echoes and subsequently compare these data to theoretical estimates calculated from single-body meteor ablation theory. All of these results show that our scattering solution provides consistent results across frequencies and a reasonable estimate of the head plasma density and line density.

4.1. UHF/VHF head plasma density comparison

We validate the scattering model by examining head echoes detected simultaneously at two frequencies. As stated earlier, we need to determine not just the profile of the head plasma, but also its size. By using two-frequency detections, we vary the head plasma size until the peak plasma density approximately matches at both frequencies. The size of the optimum head plasma is chosen to be approximately one mean free path with a dependence upon speed. Specifically, we use the modified Jones formula (Eq. (2)) to define the head plasma radius; this formula is approximately 0.023 times the Jones' (1995) formula, which incorporates head echo speed. Therefore, the head echo's altitude provides the head plasma radius. Using head plasma radius, as well as measured RCS, we subsequently interpolate on Fig. 3 to find the maximum plasma density, $n_{\max}$, for each VHF

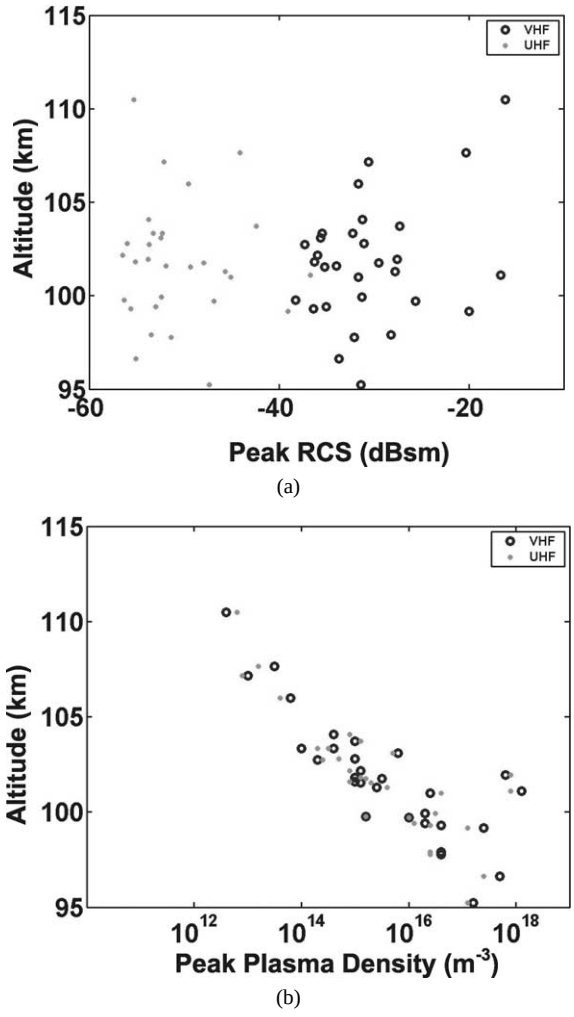

Fig. 4. (a) The maximum measured RCS from 30 head echoes detected simultaneously at VHF and UHF and (b) the maximum RCS converted to maximum head plasma density using the numerical spherical method.

head echo, and use the corresponding wavelength-dependent figures for the higher frequency (UHF, L-band) measurements.

Figure 4a shows the maximum RCS extracted from 30 head echoes detected simultaneously at VHF and UHF. We use only the maximum RCS from each head echo, so that each head echo is represented by only one point. Therefore, each meteoroid is associated with only one RCS, regardless of how extended the head echo streak is in range and time. Because a single head echo's RCS will change over its lifetime, not only from meteoroid ionization but also because it is traversing the beam, using only the maximum RCS detected at each frequency helps reduce errors due to beam pattern variations that may arise in the monopulse data. The average difference in RCS shown in Fig. 4a varies from 13.5 to 39 dBsm, which is equivalent to a difference of $22–8 \times 10^3$ m^2 between the VHF and UHF data; the VHF frequency always correlates to the higher RCS. These RCS values are consistent with those described by Zhou et al. (1998).

The RCS measurements shown in Fig. 4a are then input into the spherical scattering equations to obtain peak head plasma densities. Figure 4b contains the peak plasma density, calculated using the numerical technique, as a function of altitude for the same 30 head echoes contained in Fig. 4a. These results show that the spherical scattering solution produces approximately the same density at all altitudes, even though the measured RCS values differ by as much as 39 dBsm. We estimate the error in the spherical solution by calculating the ratio of the maximum plasma density to the minimum plasma density at each altitude. The data contained in Fig. 4b correlate to a minimum ratio of 1, and a maximum ratio of only 1.99. These ratios indicate a strong agreement between plasma densities and the self-consistency of the spherical scattering method. The peak head plasma densities of these 30 head echoes ranges from 4×10^{12} m^{-3} to 1×10^{18} m^{-3}.

We examine all of the simultaneous detections during the Leonid (1998) shower, which totals 140. Using all of the data, the minimum ratio is 1, and the largest ratio is 18.7. The median ratio is 1.9, which shows that on average, the spherical solution is producing densities that are similar to within a factor of 2.

4.2. UHF/VHF head plasma density dependence on altitude

In order to understand the dependence of head plasma density on altitude, we apply the spherical method to the maximum RCS extracted from 723 VHF and 273 UHF head echoes. Intuitively, we believe that for a single head echo, the plasma density should increase as altitude decreases, and then subsequently fall-off sharply as the meteoroid disintegrates at the lowest detected altitude. However, by extracting only the maximum plasma density from each head echo streak, we believe that the maximum head plasma density from each head echo should increase as altitude decreases, since the atmospheric density increases as altitude decreases and larger mass meteoroids will survive to lower altitudes.

We use the analytical spherical solution to determine the maximum plasma densities of 723 VHF and 273 UHF head echoes and plot these as a function of altitude. These data are shown in Fig. 5 for both the VHF (a) and UHF (b) measurements. Figure 5 shows that head plasma density decreases as head echo radius (and altitude) increases; the UHF data show a cut-off at 110 km altitude because of the smaller altitude extent used in the UHF measurements. The spherical solution produces densities from 10^{10} to 10^{18} m^{-3} at VHF, which span densities that are underdense (Mathews et al., 1997) to overdense (Pellinen-Wannberg et al., 1998) at VHF. The UHF densities vary from 10^{14} to 10^{18} m^{-3}. The UHF data are only slightly underdense, since the overdense plasma density at UHF is 2×10^{15} m^{-3}; the higher densities detected at UHF are attributed to the lower altitude extent used in the UHF system.

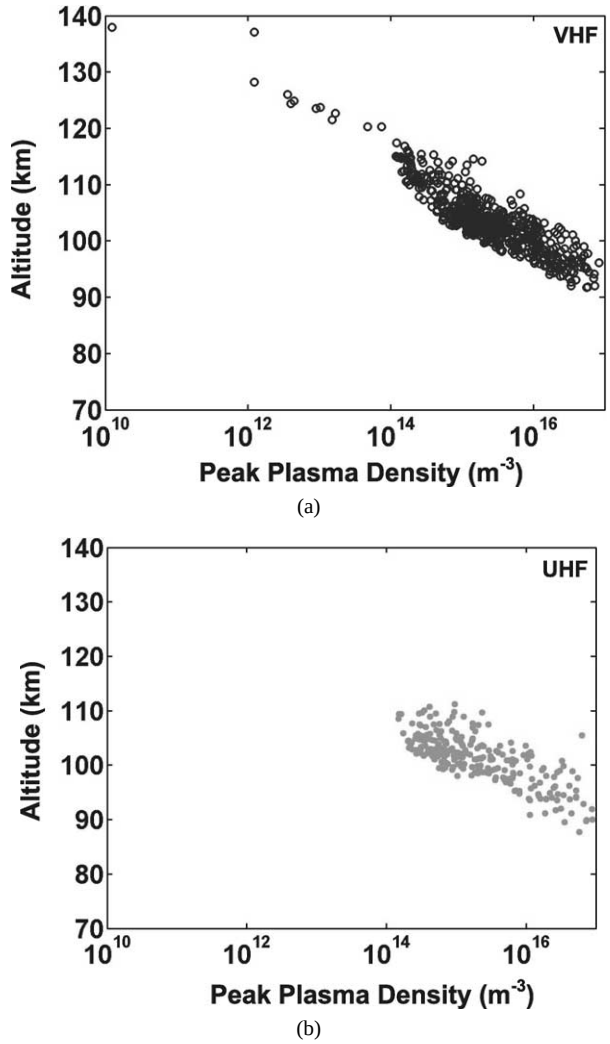

Fig. 5. Plots of maximum head plasma density, calculated using the analytical spherical solution, as a function of altitude that show that maximum density increases as altitude decreases. Each data point corresponds to the maximum measured RCS from (a) 723 VHF and (b) 273 UHF head echoes and indicates agreement between the VHF and UHF densities. The UHF data show a cut-off at 110 km altitude, which indicates the smaller altitude extent used in the UHF system.

4.3. UHF/VHF/L-band head plasma density comparison

We use the first head echo detected simultaneously at three frequencies, including VHF, UHF and L-band, to validate our method. The L-band head echo was detected by the TRADEX radar; a full description of this radar is given in (Close et al., 2002a). For this measurement, the meteoroid traversed the main beam of both the TRADEX L- and S-band system, and the ALTAIR UHF and VHF system. While the head echo was clearly located in the main beam of both the TRADEX L- and S-band beams, there was no S-band detection. Radars using C-, Ka- and W-bands also illuminated this meteor, but received no returns.

The maximum VHF head echo RCS is -10.6 dBsm at 95.75 km altitude. The maximum UHF RCS is -25.8 at

95.59 km, and the maximum L-band RCS is −36 dBsm at 95.58 km. The average 3D speed of this meteoroid is 66.5 km s^{-1}. Note that the maximum RCS occurs at progressively lower altitudes with increasing frequency.

After applying the numerical scattering model to the VHF, UHF and L-band RCS values, we obtain the following plasma densities: 1.14×10^{17} m^{-3} using VHF, 7.39×10^{16} m^{-3} using UHF, and 1.17×10^{17} m^{-3} using L-band. Note the strong agreement between the VHF and L-band plasma densities; the UHF density is within a factor of 2.

4.4. Head plasma line density comparison to single-body meteor theory

We determine the head plasma line density, q, by using the peak plasma density, $n_{\max}$, output from our scattering model; the plasma density $n(r)$ is then calculated using Eq. (1). For meteor trails, q is constant at a single altitude. For head echoes, however, q depends strongly on r and varies as a function of r up to its maximum radius, $r_{\max}$. We therefore use the average line density (q) for subsequent use in our calculations, which is given by

$$q = \frac{1}{N} \sum_{r=0}^{r=r_{\max}} n(r)\pi r^2, \tag{30}$$

where $n(r)$ is the plasma density at radius r, $r_{\max}$ is given by Eq. (2), and N is the number of steps between $r = 0$ and $r = r_{\max}$.

The ALTAIR line densities, calculated using the spherical method, are then input into the standard meteoroid mass loss equation to determine meteoroid mass

$$m = \int \frac{q\mu v}{\beta}\,\mathrm{d}t, \tag{31}$$

where m is the meteoroid mass, μ is the mean molecular mass, which is dominated by 60% oxygen and 25% silicon, v is the head echo speed and β is the ionization probability which depends upon the velocity and is given by Jones (1997). To date, Eqs. (30) and (31) have only been used with specular meteor trails, since a head echo's plasma (line) density has never been determined.

Line densities were also modeled using single-body equations of meteoroid ablation described in Hunt et al. (2004). Numerical integration of the meteoroid ablation model illustrates the relation between the initial mass, velocity, and plasma production of meteoroids as a function of altitude. Hunt et al. (2004) used a constant meteoroid mass density of 2.5 g cm^{-3} to produce modeled line densities for meteoroids with masses between 10^{-10} g and 10^{-4} g, and speeds between 11 and 72 km s^{-1}.

We calculate the ALTAIR line densities by applying the analytical spherical solution to the peak RCS taken from 723 VHF head echoes and then compare these with line densities obtained from the single-body meteoroid ablation model. The ALTAIR line densities are plotted in Fig. 6a as a function of detected altitude and meteoroid mass, which is calculated using Eq. (31); the speeds that correspond to these head echoes vary from 12 to 72 km s^{-1} where the highest speeds are detected at the highest altitudes. The line densities output from the single-body ablation model (Hunt et al., 2004) are plotted in Fig. 6b as a function of altitude and meteoroid mass as well. It is clear that the general trend between Figs. 6a and 6b is the same. As mass (and speed) increases, the maximum line density from each head echo streak increases. The smallest line densities correspond to meteoroids with low speeds and low masses, where the lowest masses are located in the upper left portion of Figs. 6a and 6b. Again, the spherical solution appears valid since it matches the theory described by the single-body ablation model rather well.

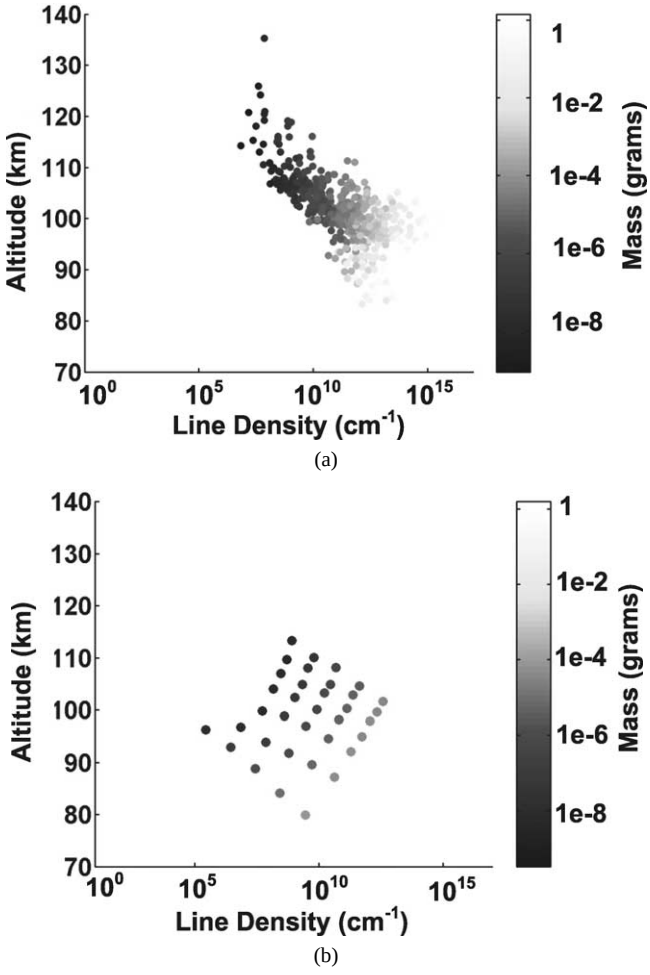

Fig. 6. (a) Maximum plasma line density calculated using the analytical scattering method as a function of altitude and meteoroid mass using the peak RCS from 723 VHF head echoes, and (b) line density as a function of altitude and meteoroid mass using the peak line density output from each meteoroid streak in the single-body ablation model. The head echo speeds used to obtain mass from line density in (a) vary from 12 to 72 km s^{-1} and are measured directly by the ALTAIR system. Note the general agreement between (a) and (b).

5. Discussion

In general, we find that the spherical solution works relatively well, since it produces similar head plasma densities using multi-frequency measurements. Given the head plasma density dependence on altitude, we can predict how head echo RCS should depend on altitude. At low altitudes, the head plasma density is large but the head plasma radius is small; at high altitudes, the plasma density is small but the plasma radius is large. The peak RCS, which indicates the strength of the signal returned from the head echo, depends upon both density and radius. Therefore, peak RCS should occur when the radius and the density together are large. Since the peak measured RCS corresponds to an altitude near 100 km (Close et al., 2002b), our hypothesis appears correct. Small RCS values will be detected at high altitudes where the plasma density is small, and also at low altitudes where the plasma radius is small. We can subsequently predict that there should be a small difference in the head echo altitude distributions detected using different frequencies. Specifically, we predict that as the radar frequency increases, the peak detection altitude of head echoes should be slightly lower in altitude to accommodate a smaller radar wavelength (for head echoes with the same 3D speed). This may explain results reported by Westman et al. (2003) and Pellinen-Wannberg and Wannberg (1994), as well as our simultaneous detections that show that peak VHF RCS, on average, occurs 270 m higher than the simultaneous UHF RCS. Note, however, that peak RCS does not necessarily correspond to peak density and might sometimes only indicate the head echo's position within the radar beam.

6. Summary and future work

A scattering method was developed and applied to meteor head echoes detected using the high-power ALTAIR radar. Head plasmas were modeled as spherically symmetric plasmas with radii that increase as altitude (mean free path) and velocity increases. The density of the head plasma was modeled as a Gaussian function. We developed a numerical solution, which was achieved by integrating Laplace's equation and using complex integration when the dielectric constant was near 0. We also derived an analytical solution, which was done by approximating the dielectric function as constant at the center of the head plasma, with a steep increase near the edge of the plasma, and using complex integration at the $\varepsilon = 0$ point. Using the spherical equations, we created a look-up table of head echo RCS as a function of head peak plasma density (plasma frequency) and head plasma radius (altitude). We subsequently interpolated on the table using the measured ALTAIR RCS and detection altitude to determine maximum head plasma density for each measured head echo.

The head plasma densities were correlated across the two-frequency measurements using 30 simultaneous detections. These data gave consistent plasma densities across frequencies, whereas the measured RCS values were quite different; this result gives confidence in the spherical solution. Head plasma densities were also plotted as a function of altitude using the peak RCS measured from 723 VHF and 273 UHF head echoes. These results showed that the maximum head plasma density from each head echo streak occurred at progressively lower altitudes, which is intuitive since larger mass meteoroids will survive to lower altitudes and produce head plasmas with higher densities. Peak detected RCS should therefore occur when the plasma is both relatively large and dense, which is consistent with peak RCS measurements near 100 km altitude. We also used a 3-frequency detection to validate the method, which produced plasma densities that were very similar across frequencies (to within a factor of 2).

Plasma densities output from our scattering model were converted to line densities and meteoroid masses using 723 VHF head echoes and their corresponding speeds. The line densities and meteoroid masses approximately matched a single-body meteoroid ablation model, which again shows that the method works relatively well.

Our future work includes developing a numerical model that does not include the electrostatic approximation, and a scattering model with a more physically realistic model of head plasma distribution. We will also refine our estimates of the ionization coefficient (β) to calculate more accurate meteoroid masses, as well as refine our estimate of the head plasma radius. By focusing on our multi-frequency measurements, we believe we can accurately determine these constants to a much greater accuracy.

Acknowledgments

The authors gratefully acknowledge the contributions from the following people: Fred McKeen, Michael Minardi, Lars Dyrud, Andy Clarke, Harry Petschek, Yakov Dimant, Gary Bust, John Mathews, Diego Janches, Peter Brown, Scott Coutts, and Phil Erickson. We also thank Ramaswamy Sridharan, Kurt Schwan and members of the Lincoln Scholars Committee for the opportunity to pursue this research. Dr. Paul Bellaire of the Air Force Office of Scientific Research under contract F19628-95-C-0002 sponsored this work. This material is also partially based on work supported by the National Science Foundation under Grant ATM-9986976.

References

Chapin, E., Kudeki, E., 1994. Radar interferometric imaging studies of long-duration meteor echoes observed at Jicamarca. J. Geophys, Res. 99, 8937–8949.

Close, S., Hunt, S., Minardi, M., McKeen, F., 2000. Analysis of Perseid meteor head echo data collected using ALTAIR. Radio Sci. 35, 1233–1240.

S0019-1035(03)00404-4/FLA AID:7281 Vol.●●●(●●●)
ELSGMLTM(YICAR):m5 2004/01/13 Prn:26/01/2004; 9:41
yicar7281
P.10 (1-10)
by:Jolanta p. 10

Close, S., Hunt, S., Minardi, M., McKeen, F., 2002a. Characterization of Leonid meteor head echo data collected using the VHF/UHF Advanced Research Projects Agency Long-Range and Tracking Radar. Radio Sci. 37, 1–9.

Close, S., Hunt, S., Oppenheim, M., Dyrud, L., 2002b. Scattering characteristics of high-resolution meteor head echoes detected at multiple frequencies. J. Geophys, Res. 107, 1–12.

Erickson, P.J., Lind, F.D., Wendelken, S.M., Faubert, M.A., 2001. Meteor head echo observations using the Millstone Hill UHF incoherent scatter radar system. In: Proceedings of the Meteoroids 2001 Conference Proceedings. In: ESA SP, vol. 495, pp. 457–463.

Evans, J., 1966. Radar observations of meteor deceleration. J. Geophys. Res. 71, 171–188.

Herlofson, N., 1951. Plasma resonance in ionospheric irregularities. Ark. Fysik 3, 247–297.

Hunt, S.M., Oppenheim, M.M., Close, S., Brown, P.G., McKeen, F.M., Minardi, M., 2004. Measurement of the meteoroid velocity distribution at earth using high power radar. Icarus. In press.

Jackson, J.D., 1975. Classical Electrodynamics. Wiley, New York.

Janches, D.J., Mathews, J.D., Meisel, D.D., Zhou, Q., 2000. Micrometeor observations using the Arecibo 430 MHz radar. Icarus 145, 53–63.

Jones, W., 1995. Theory of the initial radius of meteor trains. Mon. Not. R. Astron. Soc. 275, 812–818.

Jones, W., 1997. Theoretical and observational determinations of the ionization coefficient of meteors. Mon. Not. R. Astron. Soc. 288, 995–1003.

Jones, J., Jones, W., 1991. Oblique-scatter of radio waves from meteor trains: full-wave calculations. Planet. Space Sci. 9, 1289–1296.

Kaiser, T.R., Closs, R.L., 1951. Theory of radio reflections from meteor trails: I. J. Theor. Exper. Appl. Phys. 43, 1–32.

Mathews, J.D., Meisel, D.D., Hunter, K.P., Getman, V.S., Zhou, Q., 1997. Very high resolution studies of micrometeors using the Arecibo 430 MHz radar. Icarus 126, 157–169.

McKinley, D.W.R., Millman, P.M., 1949. A phenomenological theory of radar echoes from meteors. In: Proceedings of the IRE, pp. 364–375.

Mie, G., 1912. Grundlagen einer Theorie der Materie. Ann. Physic 37, 511–534.

Morse, P.M., Feshbach, H., 1953. Methods of Theoretical Physics, Part II. McGraw–Hill, New York.

Pellinen-Wannberg, A., Wannberg, G., 1994. Meteor observations with the European incoherent scatter UHF radar. J. Geophys. Res. 99, 11379–11390.

Pellinen-Wannberg, A., Westman, A., Wannberg, G., Kaila, K., 1998. Meteor fluxes and visual magnitudes from EISCAT radar event rates: a comparison with cross-section based magnitude estimates and optical data. Ann. Geophys. 116, 1475–1485.

Poulter, E.M., Baggaley, W.J., 1977. Radiowave scattering from meteoric ionization. J. Atmos. Terr. Phys. 39, 757–768.

Stratton, J.A., 1941. Electromagnetic Theory. McGraw–Hill, New York.

Westman, A., Wannberg, G., Pellinen-Wannberg, A., 2003. Meteor head echo height distributions and the height cutoff effect studied with the EISCAT HPLA UHF and VHF radars. Ann. Geophys. Submitted for publication.

Wyatt, P.J., 1962. Scattering of electromagnetic plane waves from inhomogeneous spherically symmetric objects. Phys. Rev. 127, 1837–1843.

Zhou, Q.H., Perillat, P., Cho, J.Y.N., Mathews, J.D., 1998. Simultaneous meteor echo observations by large aperture VHF and UHF radars. Radio Sci. 33, 1641–1654.